AIP | Journal of Applied Physics

Color tunable phosphorescence in KY3F10:Tb3+ for x-ray or cathode-ray tubes

Jinsu Zhang, Zhendong Hao, Xia Zhang, Yongshi Luo, Xingguang Ren et al.

Citation: J. Appl. Phys. 106, 034915 (2009); doi: 10.1063/1.3190511
View online: http://dx.doi.org/10.1063/1.3190511
View Table of Contents: http://jap.aip.org/resource/1/JAPIAU/v106/i3
Published by the American Institute of Physics.

Related Articles

Thermoluminescence studies on γ-irradiated Mn:Li2B4O7 single crystals
Appl. Phys. Lett. 101, 071904 (2012)

Dynamics of thermoluminescence spectra of impurity–helium condensates containing stabilized nitrogen and oxygen atoms
Low Temp. Phys. 38, 688 (2012)

Study of exciton dynamics in garnets by low temperature thermo-luminescence
J. Appl. Phys. 112, 023522 (2012)

Synthesis and phosphorescence mechanism of a reddish orange emissive long afterglow phosphor Sm3+-doped Ca2SnO4
Appl. Phys. Lett. 98, 121906 (2011)

Correlations between low temperature thermoluminescence and oxygen vacancies in ZnO crystals
J. Appl. Phys. 109, 053508 (2011)

Additional information on J. Appl. Phys.

Journal Homepage: http://jap.aip.org/
Journal Information: http://jap.aip.org/about/about_the_journal
Top downloads: http://jap.aip.org/features/most_downloaded
Information for Authors: http://jap.aip.org/authors

ADVERTISEMENT

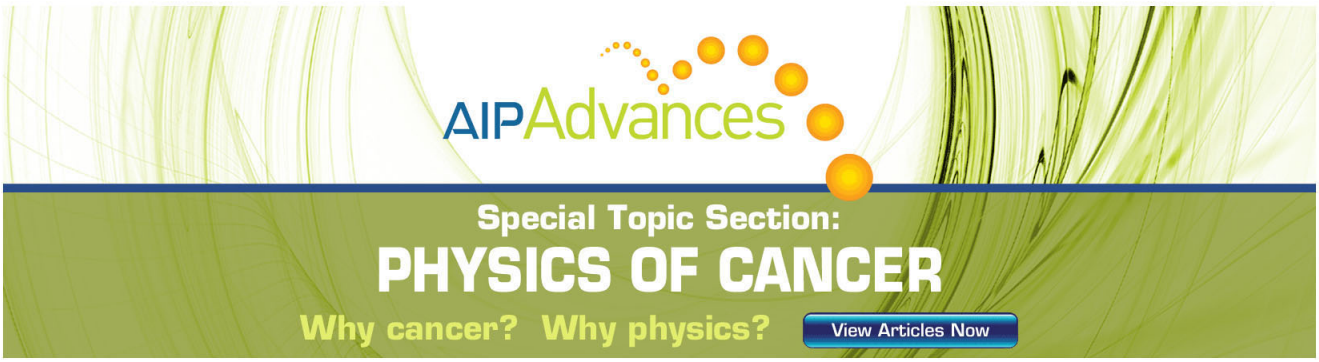

Downloaded 09 Sep 2012 to 159.226.165.151. Redistribution subject to AIP license or copyright; see http://jap.aip.org/about/rights_and_permissions

Color tunable phosphorescence in $KY_3F_{10}:Tb^{3+}$ for x-ray or cathode-ray tubes

Jinsu Zhang,[1,2] Zhendong Hao,[1] Xia Zhang,[1] Yongshi Luo,[1] Xingguang Ren,[1] Xiao-jun Wang,[1,3] and Jiahua Zhang[1,a)]
[1]*Key Laboratory of Excited State Processes, Changchun Institute of Optics, Fine Mechanics and Physics, Chinese Academy of Sciences, Changchun 130033, China*
[2]*Graduate School of Chinese Academy of Sciences, Beijing 100039, China*
[3]*Department of Physics, Georgia Southern University, Statesboro, Georgia 30460, USA*

(Received 26 May 2009; accepted 1 July 2009; published online 12 August 2009)

We report a persistent phosphor of $KY_{3(1-x)}Tb_{3x}F_{10}$ ($KY_3F_{10}:xTb^{3+}$) synthesized by solid-state reaction for x-ray or cathode-ray tubes. The phosphorescence consists of a group of blue and green emission lines originating from $^5D_3 \rightarrow {}^7F_J$ and $^5D_4 \rightarrow {}^7F_J$ transitions of Tb^{3+}, respectively. The phosphorescent emitting color can be tuned from blue to green by gradually increasing Tb^{3+} concentrations, which is attributed to the enhanced $^5D_3$-$^5D_4$ relaxation through the cross relaxation between two Tb^{3+} ions, as described by of $(^5D_3, {}^7F_6)$-$(^5D_4, {}^7F_0)$. The Tb^{3+} concentration dependent phosphorescence spectra are well simulated based on the analysis of luminescence dynamical processes using the Judd–Ofelt theory and rate equations concerning the $^5D_3$ and $^5D_4$ levels. The energy charge and release pattern of the phosphor are presented and a 10% decay time is 29 s. The measurement of the thermoluminescence glow curve gives convincing evidence for the traps analysis. © *2009 American Institute of Physics*. [DOI: 10.1063/1.3190511]

I. INTRODUCTION

Long persistent phosphors for x-ray or cathode-ray tubes have been greatly attractive due to their extensive applications.[1] One of the important applications is for displaying radar echoes on the screen due to the long period of electron beam rotation over the screen. However, a single persistent phosphor suitable for the radar tube is deficient. Therefore, two-layer phosphor screens are used in radar tubes. The first layer is made of blue emitting ZnS:Ag,Cl phosphor for cathode ray and the second layer is made of yellow-green emitting (Zn, Cd)S:Cu,Cl persistent phosphor, which is poorly cathodoluminescent but excellently photoluminescent.[2] The blue light from the first layer stimulates the second layer to emit long persistent yellow-green light. A single persistent phosphor $Zn_2SiO_4:Mn^{2+}$ containing As_2O_3 additive exhibits a emission at 525 nm, but the 10% decay time is only 150 ms, suitable for radar tubes that operated by random scanning.[3,4] Several long persistent fluoride phosphors activated by Mn^{2+} which emit orange light are also of interest.[5]

As we all know, the rare-earth ions play an important role overall system performance due to their *f-f* or *d-f* transitions. Among these rare-earth ions, the Tb^{3+} doped phosphor is well known for its high luminescence efficiency. Tb^{3+} usually emits green-sharp emission line originating from the $^5D_4$ energy level. In some cases, Tb^{3+} can also emit blue-sharp emission line originating from the higher energy level of $^5D_3$, which depends on Tb^{3+} concentration and cutoff phonon frequency of host lattices.[6] The fluoride crystalline hosts have received great attention for various luminescence fields because they have low phonon frequency for high luminescent efficiency.[7,8] The rare-earth ions doped fluoride material KY_3F_{10} with the cutoff phonon frequency of 400 cm^{-1} (Ref. 9) has been applied as a laser material due to its good optical and thermomechanical properties. The fluorescence mechanism of Tb^{3+} doped KY_3F_{10} has been investigated with a good concentration and temperature quenching properties.[10] We found that the $KY_3F_{10}:Tb^{3+}$ phosphor exhibits good long persistent phosphorescence after irradiation with x-ray or cathode-ray tubes and can be applied for the radar tubes. Different from the traditional phosphors for radar tubes, the $KY_3F_{10}:Tb^{3+}$ phosphor emits sharp lines with higher color purity and tunable emitting colors from blue to green by controlling Tb^{3+} concentrations.

In this paper, we report observation of long persistent phosphorescence in Tb^{3+} doped KY_3F_{10} as a function of Tb^{3+} concentrations after irradiation with x-ray or cathode-ray tubes. The phosphorescent emitting colors can be tuned from blue to green by gradually increasing Tb^{3+} concentrations due to the cross relaxation between two Tb^{3+} ions, as described by $(^5D_3, {}^7F_6)$-$(^5D_4, {}^7F_0)$. The Tb^{3+} concentration dependent phosphorescence spectra are well simulated.

II. EXPERIMENTAL

Powder samples of $KY_3F_{10}:Tb^{3+}$ are prepared by solid-state reaction. Tb^{3+} is considered to substitute the Y^{3+} sites. The starting material anhydrous KY, YF_3, and TbF_3 are mixed homogeneously in an agate mortar. After grounded for 1 h, the mixtures are placed in an oven at 100 °C for 12 h, and then placed in an alumina cannulation preheated at 200 °C in a pure nitrogen atmosphere for 2 h, and finally sintered at 700 °C for 8 h.

a)Author to whom correspondence should be addressed. Tel./FAX: +86-431-8617-6317. Electronic mail: zhangjh@ciomp.ac.cn.

 © 2009 American Institute of Physics

Downloaded 09 Sep 2012 to 159.226.165.151. Redistribution subject to AIP license or copyright; see http://jap.aip.org/about/rights_and_permissions

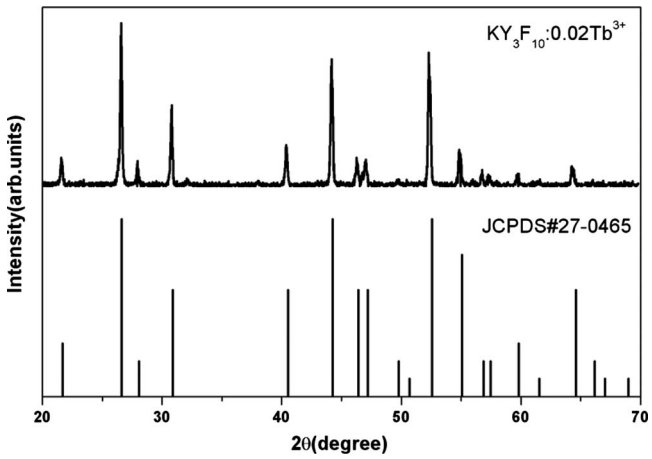

FIG. 1. XRD patterns of KY_3F_{10}:0.02Tb^{3+} samples and of the standard KY_3F_{10} pattern (Ref. 11).

The crystalline structure of the sample is investigated by the x-ray diffraction (XRD) patterns with a Cu target radiation source and a pure KY_3F_{10} phase is observed with different concentrations of Tb^{3+}. The powder XRD patterns of KY_3F_{10}:0.02Tb^{3+} is shown in Fig. 1 and has a good match with Ref. 11. A purity single powder sample was synthesized. The KY_3F_{10} crystallizes is in a face centered cubic structure belonging to the $Fm\bar{3}m(O_h^5)$ space group.[12] The Tb^{3+} occupies the Y^{3+} site with the point group symmetry of C_{4v} with the fourfold symmetry axis oriented along one of the three cubic axes.

Optical emission spectrum of $^5D_4$ to the lower ^7F_J states is detected by a boxcar-162 integrator upon excitation of the third (355 nm) harmonic of a Nd:YAG (yttrium aluminum garnet) laser. The fluorescence emission and excitation spectra are measured using HITACHI F-4500 fluorescence spectrophotometer. The long persistent phosphorescence emission spectra and time decay curves of Tb^{3+} after the x-ray excitation are measured using HITACHI F-4000 fluorescence spectrophotometer. In fluorescence lifetime measurements, the third (355 nm) harmonic of a Nd:YAG laser (Spectra-Physics, GCR 130) is used as an excitation source, and the signal is detected with a Tektronix digital oscilloscope model (TDS 3052). All of the above measurements are performed at room temperature. The thermoluminescence (TL) grow curve is measured using a TL meter with a heating rate of 1 K/s.

III. RESULTS AND DISCUSSION

A. Judd–Ofelt theory analysis

In Tb^{3+} doped KY_3F_{10} system, the de-excitation from the $^5D_3$ excited state is due to cross-relaxation, radiative, and nonradiative processes. In order to discuss the cross-relaxation process from the $^5D_3$ to $^5D_4$ energy level, the information on intrinsic optical properties including radiative and nonradiative of $^5D_3$ are required. The Judd–Ofelt theory[13,14] is employed in this section to focus on the luminescence properties of the $^5D_3$ and $^5D_4$ levels, including the branching ratios and radiative rates. The energy-level scheme of $4f^8$ configuration for Tb^{3+} in KY_3F_{10} is calculated with free ions and crystal-field parameters taken from Refs. 15–17. The nonradiative processes for $^5D_4$ can be ignored due to the large energy gap from the $^5D_4$ to the next energy level of $^7F_0$. The intensity parameters are determined basing on the measured emission spectrum and lifetime of $^5D_4$.

The electric dipole and strengths between an initial state φJ and a final state $\varphi' J'$ in the Judd–Ofelt theory is expressed as

$$S^{\mathrm{ED}}(\varphi J, \varphi' J') = \sum_{\lambda=2,4,6} \Omega_\lambda |\langle f^N \varphi J || U^{(\lambda)} || f^N \varphi' J' \rangle|, \tag{1}$$

where Ω_2, Ω_4, and Ω_6 are the Judd–Ofelt intensity parameters, $\langle f^N \varphi J|$ and $|f^N \varphi' J'\rangle$ are the initial and final states, and the matrix elements $U^{(\lambda)}$ can be calculated according to Nielson and Koster.[18]

The radiative decay rates for electric dipole transitions is expressed as

$$A(\varphi J, \varphi' J') = \frac{64\pi^4 e^2 \sigma^3}{3h(2J+1)} \chi^{\mathrm{ED}} S^{\mathrm{ED}}(\varphi J, \varphi' J'), \tag{2}$$

where $\chi^{\mathrm{ED}} = [n(n^2+2)^2]/9$ is the Lorentz local field correction factor for the electric dipole emission, the refractive index n for KY_3F_{10} is 1.490 (Ref. 19) and can be considered as a constant in the spectrum range (470–700 nm). e is the elementary charge, h is Planck's constant, and σ is the wavenumber at the emission maximum.

The radiative lifetime for the state φJ is calculated by

$$\tau_r = \frac{1}{\Sigma_{\varphi' J'} A(\varphi J, \varphi' J')}, \tag{3}$$

where the sum runs over all the radiative decay rates from the initial state φJ to the final states $\varphi' J'$.

The fluorescence branching ratios $\beta(\varphi J, \varphi' J')$ are determined by the radiative decay rates and written as

$$\beta(\varphi J, \varphi' J') = \frac{A(\varphi J, \varphi' J')}{\Sigma_{\varphi' J'} A(\varphi J, \varphi' J')} = A(\varphi J, \varphi' J') \tau_r. \tag{4}$$

The experimental data of intensities emission from the $^5D_4$ to the ^7F_J are obtained from the experimental spectrum, as depicted in Fig. 2. The lifetime of $^5D_4$ is approximately 4.7 ms obtained from the time decay measurements and can be considered as the radiative lifetime. The lifetime of $^5D_4$ for Tb^{3+} doped many materials is in the order of magnitude (millisecond).[20–22] The calculated radiative decay rates in Eq. (2), the lifetime in Eq. (3), and branching ratios in Eq. (4) with the experimental data are tabulated in Table I. The values of intensity parameters are obtained by a least-square fitting[19] between the experimental and calculated data and listed by the following:

$$\Omega_2 = 3.922 \times 10^{-20}\ \mathrm{cm}^2, \quad \Omega_4 = 0.299 \times 10^{-20}\ \mathrm{cm}^2, \quad \Omega_6 = 3.022 \times 10^{-20}\ \mathrm{cm}^2.$$

The radiative decay rates and lifetime for the $^5D_3$ are calculated by Eq. (2) and presented in Table I.

Downloaded 09 Sep 2012 to 159.226.165.151. Redistribution subject to AIP license or copyright; see http://jap.aip.org/about/rights_and_permissions

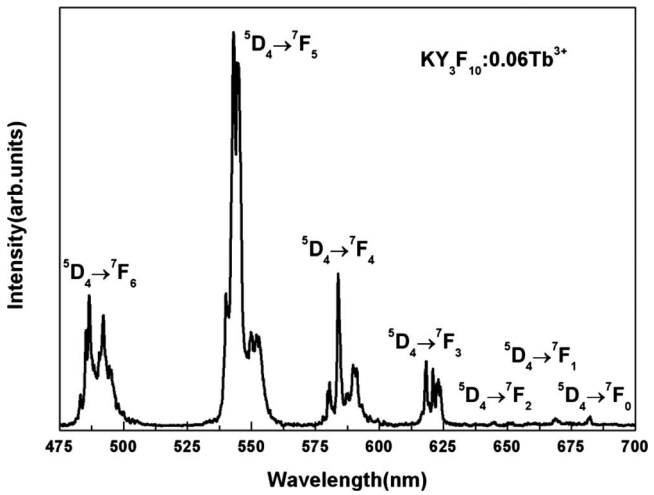

FIG. 2. Optical emission spectrum of $^5D_4$ to the lower ^7F_J states under the third (355 nm) harmonic of a Nd:YAG laser excitation.

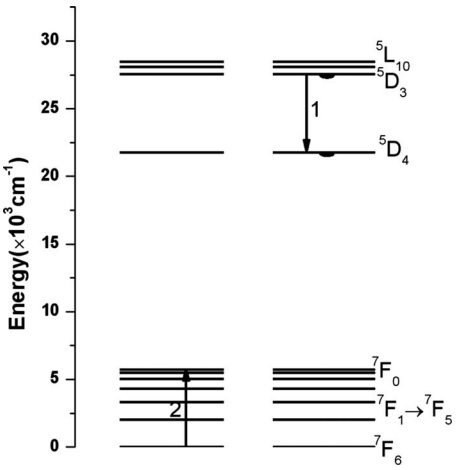

FIG. 3. Schematic energy levels of KY_3F_{10}:Tb^{3+} showing physical mechanisms for cross-relaxation energy transfer.

B. Cross-relaxation energy transfer

Figure 3 shows the schematic energy levels of Tb^{3+} in KY_3F_{10}. After the $^5D_3$ level of a Tb^{3+} ion is populated, the cross-relaxation energy transfer between the excited Tb^{3+} and another Tb^{3+} in the ground state may occur, as described by $(^5D_3, {}^7F_6)$-$(^5D_4, {}^7F_0)$. The cross relaxation speeds up the $^5D_3 \rightarrow {}^5D_4$ relaxation, resulting in two groups of emissions originating from $^5D_3$ and $^5D_4$ levels, respectively.

Figure 4 shows the excitation (λ_{em}=542 nm) and emission (λ_{ex}=218 nm) fluorescence spectra of KY_3F_{10}:0.02Tb^{3+} (solid lines) as well as its phosphorescence emission spectrum (dashed line) recorded after removal of x-ray excitation. The fluorescence and phosphorescence spectra are detected with the slits of 2.5 and 10 nm, respectively. Upon the $4f^75d$ excitation at 218 nm, there appear two groups of emissions. The blue emission lines peaking at 382, 414, and 436 nm are originating from the $^5D_3 \rightarrow {}^7F_J$ transitions, and the green emission lines peaking at 488, 542, 584, and 622 nm are from the $^5D_4 \rightarrow {}^7F_J$ transitions. It is clearly shown in Fig. 4 that the photoluminescence spectrum is consistent with the phosphorescence spectrum. The sameness is also observed in the samples with different Tb^{3+} concentrations. This means the thermal excitation for the phosphorescence is equivalent to $4f^75d$ excitation.

Figure 5 shows the phosphorescence emission spectra of KY_3F_{10}:Tb^{3+} with different Tb^{3+} concentrations after removal of the x-ray excitation, where the intensities of the green emission originating from $^5D_4$ are normalized. At low concentration of Tb^{3+}, the blue emissions from the $^5D_3$ level dominate the phosphorescence, indicating that the $^5D_3$ level is mainly populated by thermal excitation rather than the $^5D_4$ level. The intensity ratios of the green emission from $^5D_4$ to the blue emission from $^5D_3$ enhance remarkably with increasing Tb^{3+} concentrations. This is attributed to the enhancement of the cross-relaxation energy transfer among Tb^{3+} ions.

In principle, the enhanced cross relaxation can shorten the lifetime of the $^5D_3$ level, while the lifetimes of the $^5D_4$ level are unaffected if the Tb^{3+} concentration is below the quenching point.[10] In order to analyze the energy transfer rate and efficiency as a function of Tb^{3+} concentration, the fluorescence lifetimes of $^5D_3$ (τ_1) and $^5D_4$ (τ_2) for different Tb^{3+} concentrations are measured upon 355 nm pulsed laser excitation, as represented in Fig. 6. The decays of $^5D_4$ can be described as a single exponential function and the lifetimes keep around 4.7 ms. The decays of $^5D_3$ remain nonexponential function and the lifetimes are calculated according to the Inokuti–Hirayama model as the following definition:[23]

TABLE I. Experimental branching ratio and lifetime; calculated branching ratio and radiative decay rates and lifetime for $^5D_4$; calculated radiative decay rates and lifetime for $^5D_3$ in KY_3F_{10}:Tb^{3+}.

	Initial state: $^5D_4$ energy level				Initial state: $^5D_3$ energy level	
Final states $\lvert f^N\varphi' J'\rangle$	Energy Difference σ (cm^{-1})	Experimental branching ratio	Calculated branching ratio	$A(\varphi J, \varphi' J')$ (s^{-1})	Energy Difference σ (cm^{-1})	$A(\varphi J, \varphi' J')$ (s^{-1})
$^7F_0$	14 656	0.0026	0.0026	0.53	20 462	0
$^7F_1$	14 952	0.0029	0.0031	0.65	20 758	30.73
$^7F_2$	15 508	0.0026	0.0471	9.64	21 314	20.94
$^7F_3$	16 184	0.0460	0.1083	22.12	21 990	29.59
$^7F_4$	17 129	0.1219	0.1598	32.65	22 935	140.78
$^7F_5$	18 416	0.5589	0.5843	119.40	24 222	71.88
$^7F_6$	20 555	0.2650	0.0948	19.37	26 361	52.72
τ_r		4.7 ms		4.8 ms		2.88 ms

Downloaded 09 Sep 2012 to 159.226.165.151. Redistribution subject to AIP license or copyright; see http://jap.aip.org/about/rights_and_permissions

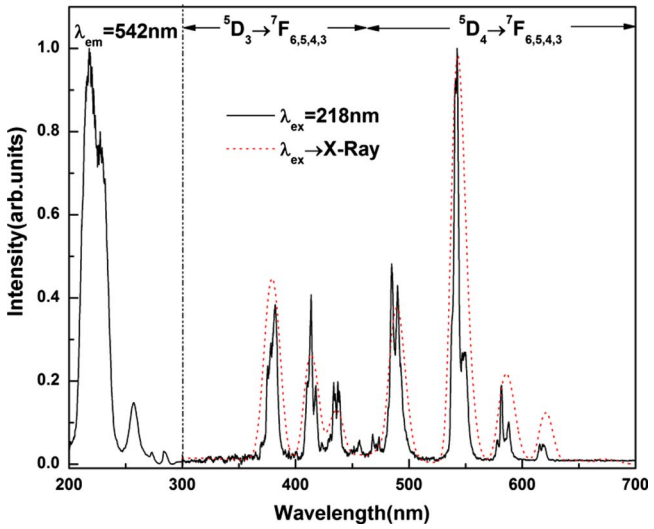

FIG. 4. (Color online) Fluorescence excitation (λem=542 nm) and emission (λex=218 nm) spectra of $KY_3F_{10}:0.02Tb^{3+}$ (solid lines) and phosphorescence emission spectrum of $KY_3F_{10}:0.02Tb^{3+}$ (dashed line) recorded after x-ray excitation.

$$\tau = \frac{1}{I_0}\int_0^\infty I(t)dt, \tag{5}$$

where I_0 is the fluorescence intensity at the time of $t=0$. The lifetimes of $^5D_3$ reduce as the Tb^{3+} concentrations increase. For the low doping sample of $KY_3F_{10}:0.0005Tb^{3+}$, the nonradiative transition for $^5D_3$ is only the multiphonon relaxation to the lower level $^5D_4$ because the Tb^{3+} concentration dependent cross-relaxation energy transfer is negligible. The lifetime of $^5D_3$ for the low doping sample is then written as

$$\tau_{10} = \frac{1}{\gamma_0 + W_0}, \tag{6}$$

where γ_0 is the radiative transition rate of $^5D_3$ and W_0 is the multiphonon relaxation rate for bridging $^5D_3$ and $^5D_4$ levels.

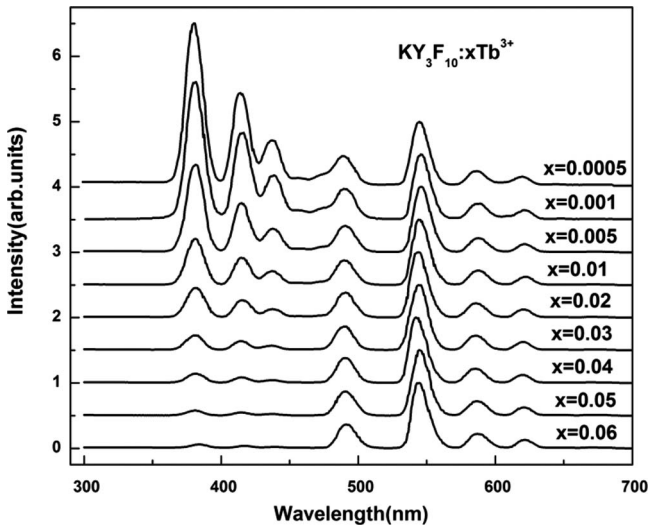

FIG. 5. Phosphorescence emission spectra of $KY_3F_{10}:xTb^{3+}$ (x=0.0005, 0.001, 0.005, 0.01, 0.02, 0.03, 0.04, 0.05, and 0.06) recorded after x-ray excitation, where the intensities of the green emission originating from $^5D_4$ are normalized.

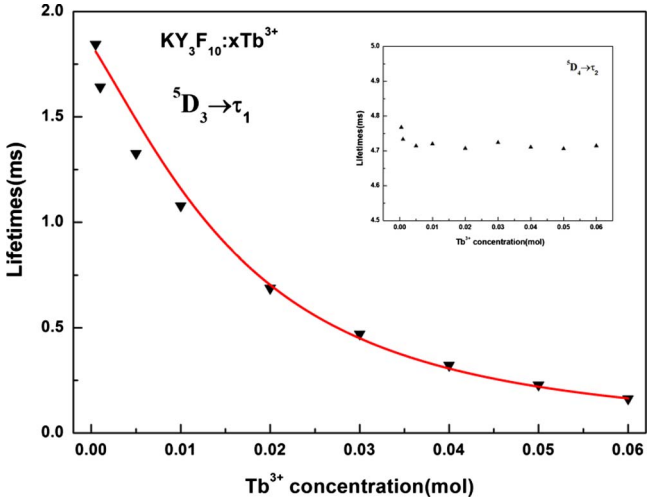

FIG. 6. (Color online) Fluorescence lifetimes of $^5D_3$ and $^5D_4$ (inside) of $KY_3F_{10}:xTb^{3+}$ (x=0.0005–0.06).

Both W_0 and γ_0 are concentration independent and γ_0 is determined using the Judd–Ofelt theory. The total radiative decay rate is 347 s^{-1}. It is observed that the measured lifetime of the $^5D_3$ is 1.84 ms in the lowest Tb^{3+} concentration sample, as shown in Fig. 6. The nonradiative decay rate for the state $^5D_3$ is 196 s^{-1} calculated by Eq. (6). The ratio of radiative decay rate to nonradiative decay rate for $^5D_3$ in our calculation is approximately 1.7:1. The nonradiative process for the state $^5D_3$ cannot be ignored. The $^5D_3$ de-excitation is due to cross-relaxation, radiative, and nonradiative processes in higher concentration samples. Then the lifetime can be written as

$$\tau_1 = \frac{1}{\gamma_0 + W_0 + W_{CR}}, \tag{7}$$

where the W_{CR} is the cross-relaxation energy transfer rate and is written, using Eqs. (6) and (7), as

$$W_{CR} = \frac{1}{\tau_1} - \frac{1}{\tau_{10}}. \tag{8}$$

According to Eq. (8), the energy transfer rates of $^5D_3$ to $^5D_4$ have been obtained and shown in Fig. 7. The energy transfer rates with different Tb^{3+} concentrations can be fitted by a quadratic relationship function of $W_{CR}=Ax^2+Bx$, implying the average energy diffusion rate between Tb^{3+} ions in the $^5D_3$ excited state not much more than the average cross-relaxation rate, where x is the Tb^{3+} concentrations; A and B are the constants for the energy transfer rate. The values of A and B are obtained by fitting the experimental data to be 1.2×10^6 s^{-1} mol^{-2} and 2×10^4 s^{-1} mol^{-1}, respectively. The calculated curve is also shown in Fig. 7 and perfectly agrees with the experimental data. The energy transfer rate increases with the increasing Tb^{3+} concentrations. The lifetimes of $^5D_3$ (τ_1) are calculated by Eq. (7) and expressed as $\tau_1=1/(Ax^2+Bx+C)$, where C is the reciprocal of τ_{10}. The calculated curve presents a good match with the experimental data, as shown in Fig. 6.

Downloaded 09 Sep 2012 to 159.226.165.151. Redistribution subject to AIP license or copyright; see http://jap.aip.org/about/rights_and_permissions

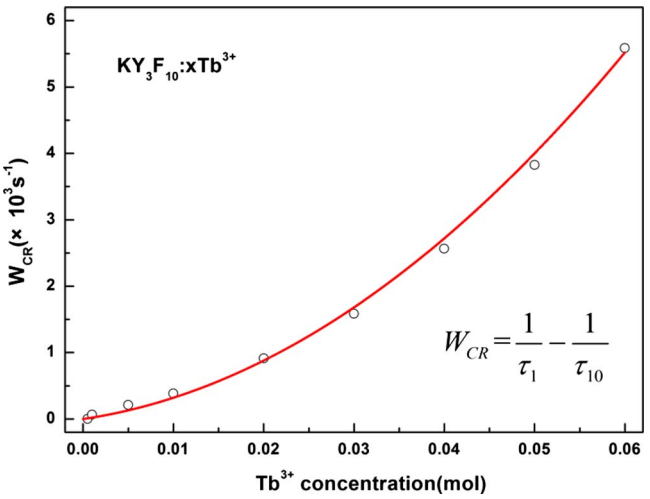

FIG. 7. (Color online) Energy transfer rates of $^5D_3$ to $^5D_4$ as a function of Tb^{3+} concentrations.

The cross-relaxation energy transfer efficiency (η_{CR}) as a function of Tb^{3+} concentrations is also observed and calculated by the following expression:[24]

$$\eta_{CR} = 1 - \frac{\tau_1}{\tau_{10}}. \tag{9}$$

The experimental data and calculated curve are shown in Fig. 8. The calculated curve shown in Fig. 8 is according to the relationship between the energy transfer rate (W_{CR}) and efficiency (η_{CR}) and expressed as $\eta_{CR}=1-1/(\tau_{10}(Ax^2+Bx)+1)$, which perfectly agrees with the experimental data. The energy transfer efficiency increases with the increasing Tb^{3+} concentrations and arrives at as high as 91%.

For the lowest Tb^{3+} concentration of 0.0005 mol, the cross relaxation is ignorable. The population of the $^5D_4$ level is only contributed by multiphonon relaxation from the upper level $^5D_3$. The rate equations describing the populations of $^5D_3$ (n_1) and $^5D_4$ (n_2) can be expressed as

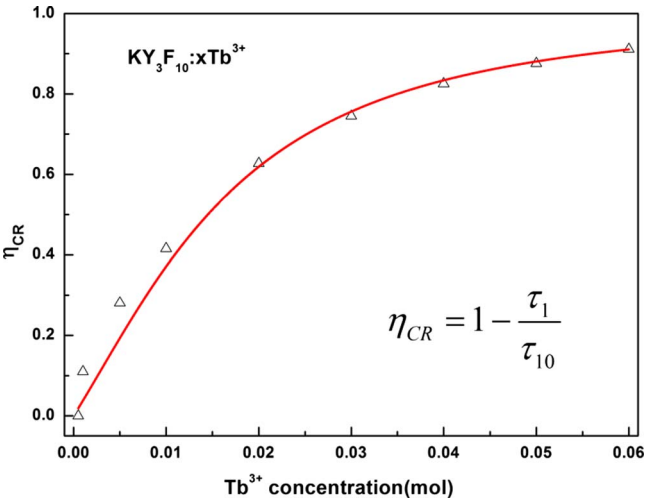

FIG. 8. (Color online) Dependence of the energy transfer efficiency on Tb^{3+} concentrations.

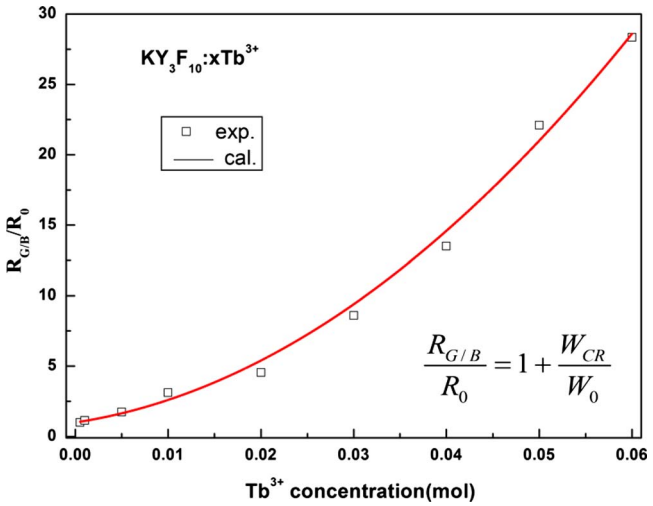

FIG. 9. (Color online) Experimental (dots) and calculated (line) ratios ($R_{G/B}/R_0$) of the blue emission from $^5D_3$ to the green emission from $^5D_4$ for different Tb^{3+} concentrations.

$$(W_0 + W_{CR})n_1 = n_2/\tau_2, \tag{10}$$

where τ_2 is the lifetime of $^5D_4$. We are interested in the intensity ratio of the green to blue emissions, $R_{G/B}$. Using Eq. (10), one has

$$\frac{R_{G/B}}{R_0} = 1 + \frac{W_{CR}}{W_0}, \tag{11}$$

where R_0 is the intensity ratio for the lowest Tb^{3+} concentration of 0.0005 mol. The experimental intensities of green emission $^5D_4 \rightarrow {}^7F_J$ and blue emission $^5D_3 \rightarrow {}^7F_J$ are directly obtained from the spectra in Fig. 5. The calculated curve by Eq. (11) with $W_{CR}=Ax^2+Bx$ and $W_0=196\ s^{-1}$ together with the experimental data are shown in Fig. 9. A perfect agreement between the experimental and calculated results is investigated.

C. Phosphorescence and thermoluminescence

Figure 10 presents the energy charge and release curves in $KY_3F_{10}:0.02Tb^{3+}$ recorded by monitoring the $^5D_4 \rightarrow {}^7F_5$

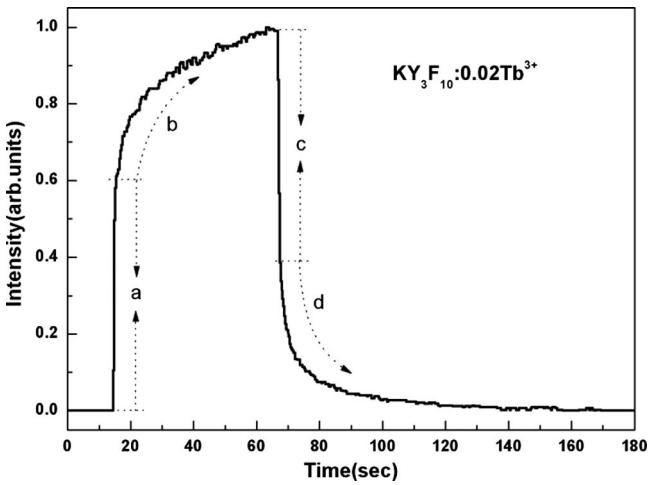

FIG. 10. Energy charge and release curves in $KY_3F_{10}:0.02Tb^{3+}$ recorded by monitoring the $^5D_4 \rightarrow {}^7F_5$ emission at 542 nm after x-ray irradiation.

Downloaded 09 Sep 2012 to 159.226.165.151. Redistribution subject to AIP license or copyright; see http://jap.aip.org/about/rights_and_permissions

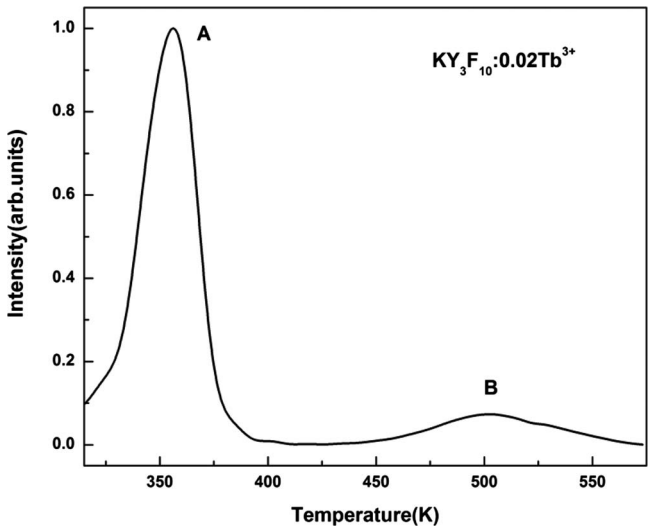

FIG. 11. TL glow curve in $KY_3F_{10}:0.02Tb^{3+}$ recorded by monitoring the $^5D_4 \rightarrow {}^7F_5$ emission at 542 nm after x-ray irradiation.

emission at 542 nm after x-ray irradiation. When the phosphor is excited, the intensity enhanced with the irradiation time before it gets saturated. Two processes are presented in the figure for the energy storage: (a) a very fast rise process is considered as photoluminescence excitation. (b) A slow rise process is considered as the energy storage for traps. After excited for 50 s, the x ray is removed. Consistent with the energy storage process, the relaxation also contains two processes: (c) a very fast decay process is considered as photoluminescence; (d) a slow decay process is for the traps to release energy. The phosphorescence decay time with 10% intensity is 29 s obtained from the process.

The TL glow curve of $KY_3F_{10}:0.02Tb^{3+}$ is measured after x-ray irradiation for 5 min, as shown in Fig. 11. Two peaks, A and B, that originated from different trapping states have been detected. For trap A, responsible for first TL peak A, is considered to be thermally released at room temperature to yield the phosphorescence. For peak A, the maximum temperature T_m and the low and high temperatures of half intensity T_1 and T_2 are 356, and 339.5, and 368.7 K, respectively. The corresponding temperatures of peak B are 502, 476.7, and 533 K, respectively. To analyze the TL parameters including the order of kinetics (b) and the activation energy (E), the factor of $\mu_g' = \delta/w$ is employed.[25,26] Where $\delta = T_2 - T_m$ and $w = T_2 - T_1$ are the high temperature and total half width, respectively. We get the values of μ_g' for peaks A and B to be 0.43 and 0.54, respectively. The factor μ_g' depends almost only on b and the relationship between μ_g' and b has been plotted.[25] The obtained order of kinetics for traps A and B are 1.1 and 2.15, respectively. Using the δ value, the activation energy can be calculated by the following expression:

$$E = c_\delta (kT_m^2/\delta), \tag{12}$$

where $c_\delta = 0.976 + 7.3(\mu_g' - 0.42)$. The activation energies for traps A and B are 0.899 and 1.30 eV, respectively. The order of kinetics of trap A is approximately 1, which means that the retrapping can be negligible. For trap B, the value of the order of kinetics indicates that a retrapping process will be considered.

IV. CONCLUSIONS

The Tb^{3+} doped KY_3F_{10} exhibiting two groups of emissions is a promising long persistent phosphor for x-ray and cathode-ray tube applications. The blue emitting is originating from $^5D_3$ and green emitting is originating from the lower $^5D_4$ energy level. The optical properties are analyzed using the Judd–Ofelt theory and a set of intensity parameters is obtained. The fluorescence branching ratio and radiative and nonradiative decay rates are predicted. Furthermore, the cross-relaxation process $(^5D_3, {}^7F_6)$-$(^5D_4, {}^7F_0)$ is discussed. The intensity ratio of blue emitting to green emitting is reduced with increasing Tb^{3+} concentrations. The experimental intensity ratio of the phosphorescence emission is consistent with the theoretical calculation basing on the fluorescence lifetime measurements. High Tb^{3+} concentrations make the distance of Tb^{3+}–Tb^{3+} shorten and thus a fast cross relaxation from $^5D_3$ to $^5D_4$ energy level. The energy transfer efficiency arrives at as high as 91% with increasing the Tb^{3+} concentrations. An ideal of 10% decay time is 29 s.

ACKNOWLEDGMENTS

This work was financially supported by the National Natural Science Foundation of China (Grant Nos. 10834006 and 10774141) the MOST of China (Grant Nos. 2006CB601104 and 2006AA03A138).

[1] S. Shionoya and W. M. Yen, *Phosphor Handbook [M]* (CRC, New York, 1998).
[2] Y. Nakanishi, H. Yamashita, and G. Shimaoka, Jpn. J. Appl. Phys. **20**, 2261 (1981).
[3] R. J. R. Bhalla and E. W. White, J. Appl. Phys. **41**, 2267 (1970).
[4] G. M. di Giacomo, J. Electrochem. Soc. **116**, 313 (1969).
[5] W. A. McAllister, J. Electrochem. Soc. **118**, 474 (1971).
[6] Z. Hao, J. Zhang, X. Zhang, S. Lu, and X. Wang, J. Electrochem. Soc. **156**, H193 (2009).
[7] Z. Kollia, E. Sarantopoulou, A. C. Cefalas, C. A. Nicolaides, A. K. Naumov, V. V. Semashko, R. Y. Abdulsabirov, S. L. Korableva, and M. A. Dubinskii, J. Opt. Soc. Am. B **12**, 782 (1995).
[8] A. Braud, S. Girard, J. L. Doualan, M. Thuau, R. Moncorgé, and A. M. Tkachuk, Phys. Rev. B **61**, 5280 (2000).
[9] P. Porcher and P. Caro, J. Chem. Phys. **68**, 4183 (1978).
[10] C. Andraud, J. P. Denis, B. Blanzat, and A. Vedrine, Chem. Phys. Lett. **101**, 357 (1983).
[11] M. P. Borzenkova, G. N. Kuznetsova, and A. V. Novoselova, JCPDS Card No. 27-0465.
[12] S. L. Chamberlain and L. R. Corruccini, Phys. Rev. B **71**, 024434 (2005).
[13] B. R. Judd, Phys. Rev. **127**, 750 (1962).
[14] G. S. Ofelt, J. Chem. Phys. **37**, 511 (1962).
[15] L. van Pieterson, M. F. Reid, G. W. Burdick, and A. Meijerink, Phys. Rev. B **65**, 045114 (2002).
[16] P. Porcher and P. Caro, J. Chem. Phys. **65**, 89 (1976).
[17] K. Heyde, K. Binnemans, and C. Görller-Walrand, J. Chem. Soc., Faraday Trans. **94**, 1671 (1998).
[18] C. W. Nielson and G. F. Koster, *Spectroscopic Coefficients for the* p^n, d^n, *and* f^n *Configurations* (MIT Press, Cambridge, 1963).
[19] P. Porcher and P. Caro, J. Chem. Phys. **68**, 4176 (1978).
[20] M. Sekita, Y. Miyazawa, and M. Ishii, J. Appl. Phys. **83**, 7940 (1998).
[21] H. P. Jenssen, D. Castleberry, D. Gabbe, and A. Linz, IEEE J. Quantum Electron. **9**, 665 (1973).
[22] M. J. Weber, T. E. Varitimos, and B. H. Matsinger, Phys. Rev. B **8**, 47 (1973).
[23] M. Inokuti and F. Hirayama, J. Chem. Phys. **43**, 1978 (1965).
[24] P. I. Paulose, G. Jose, V. Thomas, N. V. Unnikrishnan, and M. K. R. Warrier, J. Phys. Chem. Solids **64**, 841 (2003).
[25] R. Chen, J. Electrochem. Soc. **116**, 1254 (1969).
[26] S. W. S. McKeever, *Thermoluminescence of Solids* (Cambridge University Press, Cambridge, 1985), Chap. 3, p. 69.

Downloaded 09 Sep 2012 to 159.226.165.151. Redistribution subject to AIP license or copyright; see http://jap.aip.org/about/rights_and_permissions